Journal of Computational Physics **172,** 209–234 (2001)
doi:10.1006/jcph.2001.6821, available online at http://www.idealibrary.com on IDEAL®

Simple and Efficient Godunov Scheme for Computational Relativistic Gas Dynamics

I. V. Sokolov,*,† H.-M. Zhang,* and J. I. Sakai*

**Laboratory for Plasma Astrophysics, Faculty of Engineering, Toyama University, Toyama, 930-8555, Japan; and †General Physics Institute, Vavilova, 38, Moscow, 117942 Russia*

E-mail: igorsok@engin.umich.edu and sakaijun@eng.toyama-u.ac.jp

Received June 19, 2000; revised April 18, 2001

The governing equations of relativistic computational fluid dynamics (CFD) are integrated numerically. The equation of state (EOS) for a gas at relativistic temperature (the thermal energy of a gas particle is on the order of its rest mass energy) is obtained as a polynomial approximation for a gas with the Maxwellian distribution function. In contrast to previous investigations by other authors, in which the polytropic index of a gas was accepted to be constant, here the relativistic dependence of the specific heat is taken into account. The use of the proposed EOS facilitates the relativistic CFD. The Riemann invariants are expressed in terms of elementary functions so that the characteristic decomposition of the governing equations is efficient and natural. The full solution of the Riemann problem (Riemann solver) is also given by elementary functions. In order to construct it numerically, a simple transcendent equation, which relates the pressure and the velocity at the contact discontinuity, should be solved using an iteration procedure, just as in nonrelativistic CFD. So the Godunov scheme based upon the exact Riemann solver becomes simple and efficient. 1D test results are presented, as well as an example of a 2D simulation.

1. INTRODUCTION

The governing equations of computational fluid dynamics (CFD) in the usual nonrelativistic form (see, for example, [1–3]) are applicable as long as the velocity of hydrodynamic motion is much less than the speed of light. If the velocity of motion is comparable to the speed of light, then the relativistic equations of motion are valid [1].

To complete the equations of motion, the equation of state (EOS) should be used. The EOS for a gas with the constant polytropic index κ is surely the most popular model in *nonrelativistic* CFD. It is a physically reasonable model which fits the actual parameter dependencies for real gases within wide ranges of pressure, density, and temperature. On

0021-9991/01 $35.00

the other hand, this model also facilitates computations. A pressure may be readily expressed in terms of an energy density, and vice versa; the Riemann invariants are simple and may be computed efficiently. The Roe-averaged state may be easily constructed. The solution of the Riemann problem (Riemann solver—RS) may be computed by solving numerically the simple transcendent equation, which relates the velocity and the pressure at the contact discontinuity, so the Godunov numerical scheme is simple and efficient.

Again, the attractive features of the EOS with the constant polytropic index, such as good conformity with the actual behaviour of the physical parameters of real matter and the possibility of facilitating the computations efficiently, are valid only for nonrelativistic CFD as long as the equations themselves are valid. At relativistic temperatures another EOS should be found which has the same attractive features as applied for *relativistic* CFD. The purpose of the present paper is to find such an EOS and to use it in constructing the Godunov scheme.

Relativistic CFD has been developed in the past two decades mainly for astrophysical applications. However, recent progress in the development of extremely powerful table-top lasers has resulted in the appearance of a new *laboratory* object, which can also be simulated using relativistic CFD, namely, a super-bright laser pulse propagated through the plasma. The focused laser intensity may be so high that the velocity of the plasma-particle-driven motion may be comparable to the speed of light for electrons and even for ions. An example of the simulation of the super-bright laser pulse propagation through the channel was reported in [4] with the use of the numerical scheme described in the present paper.

In most papers, the equations of relativistic CFD are numerically integrated on an Eulerian grid using the finite volume method [5–10]; today, it is advanced using modern high-resolution shock-capturing (HRSC) methods [11–16] (see also the recent review paper [17] and the papers cited there). Here we consider only the conservative Godunov schemes, so that all the nonconservative schemes, such as the Glimm [18] method and quasi-linear formulations [19], are beyond our scope.

The simulations based on all known algorithms for relativistic CFD usually are rather sophisticated. Even the use of the approximate Riemann solver (see [14, 19]) or simplified TVD flux [20] still results in schemes which are much more complicated than their analogs for common nonrelativistic CFD.

From a formal point of view both nonrelativistic and relativistic CFD belong to the class of hyperbolic systems of conservation laws,

$$\frac{\partial \mathbf{U}}{\partial t} + \frac{\partial \mathbf{F}_j(\mathbf{U})}{\partial x_j} = 0, \tag{1}$$

which, generally speaking, may be numerically integrated by just the same methods [2, 3]. Moreover, the relativistic CFD equations may be reduced to literally the same form as those for nonrelativistic CFD. Nevertheless, in relativistic CFD the function $\mathbf{F}_j(\mathbf{U})$ is usually implicit, or, equivalently, the recovery procedure for the primitive variables, such as the pressure and the velocity, appears to be implicit. That is why even in using the explicit scheme for time integration, the iterative calculations should be performed in computing the hydrodynamic flux.

The most advanced numerical schemes for nonrelativistic CFD are based upon the exact RS for hydrodynamic equations (see [2, 3]). The recent investigations [21, 22] show that in relativistic CFD the construction of the Riemann solver can only be

reduced to numerical integration of an ordinary differential equation. The numerical scheme based on this approach can hardly be efficient, because the CPU time consumption increases.

Simple analysis shows that many difficulties with relativistic CFD come from the use of the EOS with a constant polytropic index $\kappa = 5/3$ or $\kappa = 4/3$. First, this EOS is not applicable to the description of matter in relativistic motion, because the specific heat in this motion cannot be considered constant. It is well known (23, the problem in paragraph 44) that the specific heat of a gas at ultrarelativistic temperature is twice as high as that of one at a lower (nonrelativistic) temperature. Hence the polytropic index is not constant either. The dependence of the specific heat on the temperature is a direct consequence of the relativistic dependence of the particle energy upon its momentum; thus the EOS with the constant polytropic index appears to be in direct contradiction to a relativity principle.

This contradiction might be overlooked if at least the EOS with a constant polytropic index facilitated the computations. On the contrary, this unrealistic EOS appears to be one of the main sources of complexity for relativistic CFD. The difficulties in *numerical* simulations which come from the EOS having no *numerical* accuracy seem to be unreasonable.

Since we are dealing with a physical problem, rather than starting from a well known mathematical model, we suggest a special form of the equation of state (EOS) for matter at relativistic temperature. The new EOS is much more realistic and practically coincides with the EOS of a gas with a relativistic Maxwellian distribution function [24]. Actually we are proposing nothing more than a kind of polynomial approximation for a well established physical model. Nevertheless this approach drastically facilitates the procedure for flux computation. Riemann invariants are given by *ordinary functions*, while for the generally accepted EOS they must be found by solving an *ordinary differential equation*. When this EOS is introduced, relativistic CFD becomes as simple as nonrelativistic CFD.

Thus, in the present paper, we show that in the case of an appropriate choice of a relativistic EOS, the hydrodynamic description of the fluid motion becomes more reliable because the equation proposed is more exact than the EOS for polytropic gas. On the other hand, the relativistic hydrodynamic equations with this EOS become quite analogous to those for nonrelativistic hydrodynamics, and their numerical integration is strongly facilitated, because any traditional scheme (sometimes even the existing code) for nonrelativistic CFD may also be applied to relativistic CFD with tiny changes. In particular, the Riemann invariants and the RS are simple and may be efficiently used in computations. The Godunov scheme described here is only one of the possible HRSC schemes.

The layout of the paper is as follows. In Section 2 we first rewrite the governing equations of relativistic CFD as a hyperbolic system of conservation laws which coincides with nonrelativistic hydrodynamics; then in Section 3 we suggest a new form of the equation of state (EOS) and show its physical advantage and computational efficiency. The relations between the conserved variables and the primitive ones are briefly discussed in Section 4. We also rewrite the governing equations in a characteristic form and give the formulae for Riemann invariants in Section 5. Rankine–Hugoniot relations are given in Section 6. The solution of the Riemann problem scheme is described in Section 7. In Section 8, we present the test results for the Godunov scheme.

2. THE GOVERNING EQUATIONS IN THE FORM OF CONSERVATION LAWS

The equations of relativistic hydrodynamics may be written in the form of conservation laws (see [1]) as a condition for the 4-divergence of the momentum–energy tensor T_i^k to be equal to zero:

$$\frac{\partial T_i^k}{\partial x^k} = 0. \tag{2}$$

Using the space and time derivatives, one can rewrite Eq. (2) as the energy equation

$$\frac{1}{c}\frac{\partial T^{00}}{\partial t} + \frac{\partial T^{0\alpha}}{\partial x_\alpha} = 0, \tag{3}$$

as well as the momentum equation

$$\frac{1}{c}\frac{\partial T^{0\alpha}}{\partial t} + \frac{\partial T^{\alpha\beta}}{\partial x_\beta} = 0. \tag{4}$$

The components of the energy–momentum tensor are (see [1])

$$T^{\alpha\beta} = \frac{w v_\alpha v_\beta}{c^2(1 - v^2/c^2)} + P\delta_{\alpha\beta}, \quad T^{0\alpha} = \frac{w v_\alpha}{c(1 - v^2/c^2)}, \quad T^{00} = \frac{w}{1 - v^2/c^2} - P, \tag{5}$$

where w is the enthalpy density in a local rest framework (in which the given small volume of the fluid is at rest), v_α is the three-dimensional velocity vector, $\delta_{\alpha\beta}$ is the unit tensor, and P is the pressure. Below the speed of light, c is accepted to be equal to unity, which may be ensured by an appropriate choice of units for time and the spatial coordinates.

If the number of particles is conserved, which is true at least in the limit of a low (nonrelativistic) temperature, then the conservation law for the density is given by the equation [1]

$$\frac{\partial}{\partial t}\frac{r}{\sqrt{1 - v^2}} + \frac{\partial}{\partial x_\alpha}\frac{r v_\alpha}{\sqrt{1 - v^2}} = 0, \tag{6}$$

where r is the density in a local rest frame of reference.

At an ultrarelativistic temperature, Eq. (6) becomes invalid, because the particle number is no longer conserved, or more precisely, Eq. (6) is valid as an equation for variable r which has no longer a sense of the rest mass density in this limit. This difficulty is irrelevant if the physically correct EOS is used, because in a universal ultrarelativistic EOS the pressure does not depend upon r and Eq. (5) becomes mathematically independent of Eq. (6). Below we consider the requirement for the EOS to be independent of r at high temperature (more exactly, the pressure should be a function of w only) as one of the necessary conditions to be fulfilled in choosing the EOS. Otherwise not only the EOS, but even the governing equations are not well founded.

On introducing the Lorentz factor γ, mass density ρ, and enthalpy density h, as well as the effective density $\tilde{\rho}$,

$$\gamma = \frac{1}{\sqrt{1 - v^2}}, \quad \rho = r\gamma, \quad h = w/r, \quad \tilde{\rho} = \frac{r}{h}, \tag{7}$$

Eqs. (3), (4), and (6) may be rewritten in a form which coincides with nonrelativistic hydrodynamics,

$$\frac{\partial}{\partial t}\begin{pmatrix}\rho\\ \mathbf{J}\\ E\end{pmatrix}+\frac{\partial}{\partial x_\alpha}v_\alpha\begin{pmatrix}\rho\\ \mathbf{J}\\ E\end{pmatrix}+\frac{\partial}{\partial x_\alpha}P\begin{pmatrix}0\\ \delta_{\alpha\beta}\\ v_\alpha\end{pmatrix}=0, \tag{8}$$

where

$$\mathbf{J}=\frac{\rho^2}{\tilde{\rho}}\mathbf{v},\quad E=\frac{\rho^2}{\tilde{\rho}}-P, \tag{9}$$

J being the momentum density.

To close the system of conservation laws, the *primitive* variables, namely, the velocity vector and the pressure, should be expressed in terms of the conserved variables. To do this we have to employ an EOS, which relates the thermodynamic pressure to some other thermodynamic parameters which in turn should be expressed in terms of some combinations of the conserved variables.

Two important points should be mentioned here. First, only Lorentz invariant combinations of the conserved variables can be used to find the thermodynamic parameters, such as

$$h^2=\frac{(E+P)^2-\mathbf{J}^2}{\rho^2},\quad \tilde{\rho}=\frac{\rho^2}{E+P}, \tag{10}$$

because any thermodynamic parameter is Lorentz invariant. Second, it appears that *any* Lorentz invariant combination of the conserved variables *must* involve nonconserved variable(s) also. In Eq. (10) the pressure is present in the right-hand side; the other Lorentz-invariant combinations can involve h, r, or $\tilde{\rho}$. That is why the procedure for finding the pressure in relativistic CFD is usually implicit.

According to Eq. (10), it is convenient to consider the pressure in relativistic CFD as a given function of h^2 and $\tilde{\rho}$, i.e., to use a relativistic EOS in a form as follows:

$$P=\tilde{P}_{rel}(h^2,\tilde{\rho}). \tag{11}$$

As long as the EOS $\tilde{P}_{rel}(h^2,\tilde{\rho})$ is given, the pressure can be recovered from the conserved variables by solving the equation, resulting from Eqs. (10)–(11),

$$P=\tilde{P}_{rel}\left(\frac{(E+P)^2-\mathbf{J}^2}{\rho^2},\frac{\rho^2}{E+P}\right). \tag{12}$$

The velocity vector may then be found as follows:

$$\mathbf{v}=\frac{\mathbf{J}}{E+P}. \tag{13}$$

The hyperbolic system of conservation laws (Eq. (8)) coupled with the equations for recovering the primitive variables (Eqs. (12 and 13)) is closed and may be numerically solved using any conservative scheme developed for this kind of system [2, 3]. Moreover, the conservative equations for relativistic CFD and for nonrelativistic CFD fully coincide; only the equations for primitive variables differ. In nonrelativistic CFD the pressure may

be considered as a function $\tilde{P}_{nr}$ of the (Galilean-invariant) density and the internal energy density e, which can be expressed in terms of the Galilean-invariant combination of the conserved variables $e = E - \mathbf{J}^2/(2\rho)$ (the total energy E in nonrelativistic CFD does not involve the rest mass energy!), so that Eqs. (12) and (13) become

$$P = \tilde{P}_{nr}(\rho, E - \mathbf{J}^2/(2\rho)) \tag{14}$$

$$\mathbf{v} = \frac{\mathbf{J}}{\rho}. \tag{15}$$

Comparing Eqs. (12) and (13) with Eqs. (14) and (15), we see that the difference between nonrelativistic and relativistic CFD generally is not more essential than the difference between nonrelativistic CFD using different equations of state. On the other hand, the particular choice of the EOS which allows the numerical analysis to be simplified, is different for relativistic and nonrelativistic CFD, because Eq. (12) differs from Eq. (14).

3. INTERPOLATED EQUATION OF STATE

Let us first discuss the general requirements for the relativistic EOS. For a relativistic temperature the fluid may normally be considered as an ideal gas. In addition the conserved particle density governs the pressure of gas at least for moderate temperature. Thus the gas EOS may be used in the generally accepted form

$$P = r f(h), \tag{16}$$

where the temperature $f = T/m$ related to the rest mass energy of one particle may be considered a function of the enthalpy per unit mass.

This expression is quite general and valid for any ideal gas. The specific heat at the constant pressure related to one particle is given by the general formula

$$c_P = \frac{d(w/r)}{d(T/m)} = \frac{dh}{df}. \tag{17}$$

For the sake of simplicity, the particular case of a gas with a constant specific heat had been used in most of the previous papers on relativistic CFD. Taking into account the condition $h \to 1$ as $T \to 0$ (the enthalpy density tends to the rest mass energy in this limit), one can obtain the usual EOS with a constant specific heat

$$f(h) = \frac{h-1}{c_P}, \quad c_P = const. \tag{18}$$

This EOS is commonly used in relativistic CFD for $c_P = 5/2$ (polytropic index is $\kappa = 5/3$) or $c_P = 4$ ($\kappa = 4/3$).

However, the frequently used EOS (18) is only one of many possible choices and may not be the best one. On one hand, Eq. (18) cannot even be considered an *approximation* for a realistic EOS (see Fig. 1), since the two cases $\kappa = 5/3$ and $\kappa = 4/3$ only give reasonable upper and lower *bounds* for it. An ultrarelativistic limit of Eq. (18) is also doubtful. These facts are not surprising because it is well known that the specific heat at constant volume, $c_V = c_P - 1$, at ultrarelativistic temperature is twice that at low (nonrelativistic) temperature (see [23], the problem in paragraph 44). Thus the assumption that $c_P = const$ for matter

at relativistic temperature contradicts physical principles. On the other hand, the choice of an EOS in the form of Eq. (18) does not facilitate theoretical analysis and numerical simulations at all. Such a choice facilitates Eq. (16), rather than Eq. (12), which is actually to be solved.

In fact the model of gas with $c_P = const$ is the basic model for *nonrelativistic* CFD, because for common nonrelativistic gases this model, first of all, is sufficiently accurate. Second, this model facilitates computation. Equation (14) can be easily solved, so the pressure may be easily expressed in terms of the density and the energy density, or the same primitive variables may be expressed in terms of the conserved ones. The Roe-averaged state may be easily found, so that total variation diminishing (TVD) numerical schemes are efficient. The Riemann invariants are simple functions of primitive variables. Hugoniot relations at the fronts of shock waves are also very simple and are computed efficiently, so the Riemann solver is efficiently constructed, as the base for the Godunov scheme and others (see [2, 3]). But, again, these considerations are valid only for nonrelativistic CFD.

Now our purpose is to find the EOS for *relativistic* CFD which has the same advantages as the EOS with $c_P = const$ for nonrelativistic CFD. We require that this EOS be exact enough within a wide range of physical parameters, and that the relativistic CFD which is based on this EOS be easy and efficient. Here we show that such an EOS does exist and moreover that it differs from Eq. (18).

Rather general and simple considerations allow us to establish the form of the EOS. First, the form of Eq. (16) seems to be mandatory, so only the function $f(h)$ may be the subject of choice. Then for cold matter the enthalpy involves only the input from the rest mass energy, so the requirement $f \to 0$ as $h \to 1$ should be fulfilled for massive matter.

For an ultrarelativistic temperature, the EOS is well established theoretically. If particle–antiparticle pairs are created intensely via the particle collisions, or if the main input to the enthalpy is due to radiation energy, or if the thermal energy of the particles is much greater than their rest mass energy—in all these cases the universal ultrarelativistic EOS is given by the formula [1, 23]

$$P = \frac{w - P}{3} = \frac{w}{4}. \tag{19}$$

As we have already mentioned, the dependence upon r vanishes from the EOS at this limit. Equations (3)–(5) are closed by Eq. (19) and become independent of the equation for density at relativistic temperature. The latter equation may even be invalid, because in pair creation the rest mass energy is not conserved. Thus the necessary physical requirement for the EOS to have a correct ultrarelativistic limit is given by the condition $f \to h/4$ as $h \to \infty$. It should be mentioned that the best choice among the equations of state is Eq. (18) for $c_P = 4$ ($\kappa = 4/3$), which still gives the EOS $P = \frac{1}{4}(w - r)$, which does not coincide with Eq. (19), although the specific heat in Eq. (19) is the same: $c_P = 4$.

This is why a reasonable interpolated formula for f may be proposed which embraces both of two limiting cases,

$$f(h) = ah - b/h, \tag{20}$$

where $a = const$ and $b = const$.

In any conservative numerical scheme for relativistic CFD, the EOS is applied to computing the numerical flux via the interface between the two adjacent cells, so the values of a and b should be considered to be constant only within the comparatively narrow ranges of the physical parameters governed by two rather close sets of hydrodynamic variables in the two adjacent cells. It is obvious that by using *two* fitting constants one can readily approximate any physically reasonable EOS within the narrow range of parameters and take into account any interesting physical effects, such as the presence of two or more sorts of particles, radiation, etc.

It is also interesting to consider the simplest possible EOS, Eq. (20), in case the fitting constants a and b are actually constant and do not depend on h at all. Then the condition $f \to h/4$ as $h \to \infty$ gives $a = 1/4$, and the condition $f \to 0$ as $h \to 1$ gives $a = b$, so that the EOS becomes

$$f(h) = \frac{1}{4}\left(h - \frac{1}{h}\right). \tag{21}$$

We thus obtain the simplest possible EOS which meets all general physical requirements. This EOS dramatically facilitates both theoretical analysis and computations in relativistic CFD. Here we show that the theoretical advantage of such an approach does not come at the cost of accuracy. For a physical model of a gas, of particles with the same rest mass energy m, such as a nondegenerated electron–positron plasma, the condition of thermodynamic equilibrium results in a well known EOS, which almost coincides with Eq. (21), the discrepancy being surprisingly small.

Indeed the ideal one-fluid hydrodynamics considered here is appropriate only for the description of gas motions in which the gas is close to local thermodynamic equilibrium. As a result of the condition of thermodynamic equilibrium the distribution function of such a gas is Maxwellian. On averaging the particle energy over a relativistic Maxwellian distribution function (see problem 2 in paragraph 38 in [23]), one can readily represent the enthalpy h as a function of the temperature $T/m = f$ as

$$h = 4f + \frac{K_1(1/f)}{K_2(1/f)}, \tag{22}$$

where $K_1(z)$ and $K_2(z)$ are modified Bessel functions of the second kind (McDonald functions, which also may be reduced to Hankel functions with imaginary arguments). Equation (22) may be also derived using Eqs. (235) and (231) in [24, p. 396].

Equation (22) has been used in some papers for fine relativistic CFD simulations (see, for example, [25]) resulting in further sophistication of the flux computation procedure. It appears that our simplest EOS, Eq. (21), ensures a surprisingly good approximation for the function Eq. (22).

In Fig. 1 the curve represents the theoretical EOS, Eq. (22), which is valid for moderately relativistic temperatures. The ultrarelativistic Eq. (19) is also shown as a theoretical limit for very high temperatures. Interpolated EOS Eq. (21) is displayed as a solid curve. This curve matches very well with the curve for Eq. (22) and also has correct asymptotic behavior at the ultrarelativistic limit. Thus our interpolated EOS is rather close to a physically reasonable model of the gas with a relativistic Maxwellian distribution function.

The dependencies for commonly accepted EOS Eq. (18) with a constant polytropic index are shown by two straight lines for $\kappa = 5/3$ and $\kappa = 4/3$. One can see that such an EOS

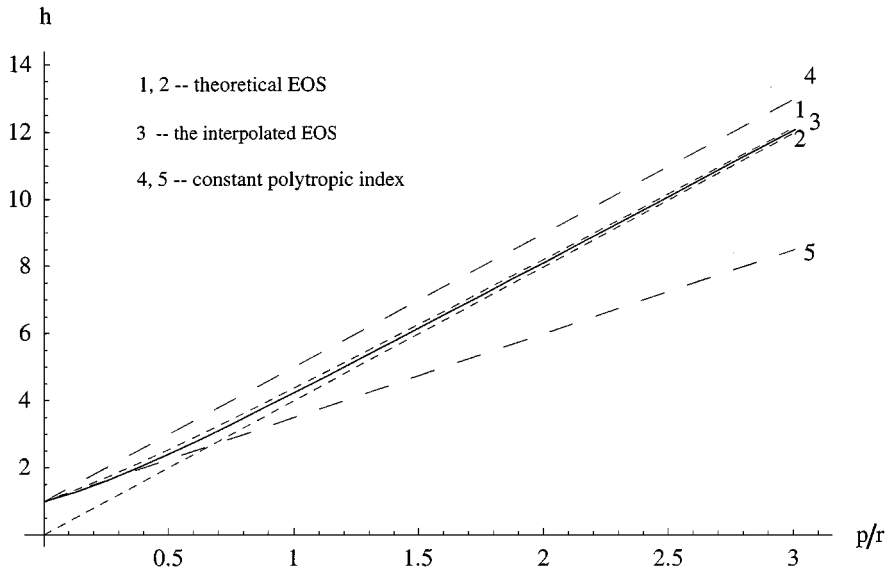

FIG. 1. The dependence f(h) for different equations of state. Curve 1: $h = 4f + \frac{4K_1(1/f)}{K_2(1/f)}$—exact relativistic EOS for an ideal gas with the Maxwellian distribution function. Line 2: $f = \frac{h}{4}$—the universal ultrarelativistic EOS. Curve 3: $f = \frac{h}{4} - \frac{1}{4h}$. Lines 4 and 5, $f = \frac{1}{4}(h-1)$ and $f = \frac{2}{5}(h-1)$, respectively, correspond to the constant value of polytropic indexes $\kappa = \frac{4}{3}$ and $\kappa = \frac{5}{3}$.

cannot be considered accurate, so the difficulties arising from use of this EOS (see below) are not compensated.

In all the formulae in the present paper, the values $a = b = 1/4$ are implied, corresponding to the choice of the EOS in a form of Eq. (21). Nevertheless, all the derivations are fulfilled for the more general case of Eq. (20).

More strict theoretical analysis shows that at rather low, essentially nonrelativistic temperature $T \ll 0.1$ m, there is some distinct discrepancy between the values of the *derivative* of function $f(h)$ (rather than in the values of the function itself) for the interpolated EOS and for the theoretical EOS. Namely, the interpolated EOS, Eq. (21), gives the low-temperature limit value for the specific heat as $c_P \to \frac{1}{2a} = 2$ as $h \to 1$ (a formula

$$\kappa = \frac{c_P}{c_P - 1} \to \frac{1}{1 - 2a} \tag{23}$$

establishes the correspondence with the nonrelativistic limit and is used below). The value $c_P = 2$ corresponds to the polytropic index $\kappa = 2$ that is pertinent to astrophysical plasmas in a magnetic field. In the absence of the magnetic field the value of c_P may actually be a little bit higher ($c_P = 5/2$ instead of $c_P = 2$); nevertheless the difference is unimportant and is ignored here. Otherwise, due to the presence of two fitting constants in interpolated EOS Eq. (20), for more accurate simulations one can allow a and b to be slowly varying functions of h, tending, for example, to $1/5$ at lower temperatures and to $1/4$ at higher temperatures. Then the specific heat at low temperature becomes $c_P = 5/2$; any other physically reasonable value may also be achieved using different values of fitting parameters a and b and at the cost of slightly degrading efficiency.

4. PRIMITIVE VARIABLES RECOVERY BY USE OF THE INTERPOLATED EOS

Using the interpolated EOS, Eq. (20) the procedure for computing the primitive variables and then the flux becomes simple and straightforward. On representing the general gas EOS, Eq. (16), in the form of Eq. (11), one can readily reduce Eq. (12) to the equation for finding $\Pi = E - P$ as follows:

$$\Pi^2 - \Pi E - \rho\sqrt{\Pi^2 - \mathbf{J}^2}\, f\left(\frac{1}{\rho}\sqrt{\Pi^2 - \mathbf{J}^2}\right) = 0. \tag{24}$$

Now the crucial nature of the choice of the EOS becomes obvious. With the usually accepted EOS with a constant polytropic index Eq. (24) becomes irrational and may be solved only by using an iteration procedure or may be reduced to a fourth order algebraic equation. In this way it is difficult to ensure that the velocity is subluminal due to finite error of iterations; the code becomes more complicated and CPU time-consuming.

On the contrary, on using the interpolated EOS, Eq. (20), the Eq. (24) becomes

$$(1-a)\Pi^2 - \Pi E + a\mathbf{J}^2 + b\rho^2 = 0, \tag{25}$$

and then it can be explicitly solved:

$$P = \Pi - E = \frac{1}{2(1-a)}\left\{\sqrt{E^2 - 4(1-a)(a\mathbf{J}^2 + b\rho^2)} - (1-2a)E\right\}. \tag{26}$$

For the simplest interpolated EOS, Eq. (21), one can put $a = b = 1/4$ into Eqs. (25) and (26).

This equation should be solved only for the physically compatible set of the conserved variables. Since the total energy must not be less than the rest mass energy, i.e., $h^2 \geq 1$, and $P \geq 0$, the first of Eqs. (10) gives

$$E^2 \geq \left(\mathbf{J}^2 + \frac{b}{a}\rho^2\right), \tag{27}$$

resulting in $\Pi^2 \geq E^2 > \mathbf{J}^2$ and then $\mathbf{v}^2 < 1$, $P \geq 0$. For exact values of the conserved variables the condition Eq. (27) is a direct consequence of the pressure positivity; nevertheless, for approximate values of the conserved variables, obtained from numerical simulations, checking the condition Eq. (27) is sometimes worthwhile. Its fulfillment automatically ensures both the positivity of pressure and the subluminal value of velocity (see Eq. (13)).

It is also worth mentioning that the requirement that the velocity be subluminal is weaker than a pressure positivity condition, so if the scheme is positively conservative [26], this ensures the relativistic property of the velocity in relativistic CFD. We see that having a numerical scheme that is positive conservative, which strongly depends upon the choice of the first order monotone numerical (see [26] for more detail), is of greater importance for relativistic CFD. The Godunov scheme is proven to have this property, which is an additional argument in favor of it.

5. CHARACTERISTIC FORM OF THE RELATIVISTIC CFD EQUATIONS

The advantage of the interpolated EOS becomes even more important as we proceed to the construction of truly HRSC schemes. The first step in this process is to construct

a characteristic decomposition of the governing equations and represent them in a form $\partial R_i/\partial t + \lambda_i(\partial R_i/\partial x) = 0$, and to find the Riemann invariants R_i and the characteristic speeds λ_i. These building blocks are used in the Godunov scheme, the Osher scheme, and almost all the other high-resolution schemes to some extent.

While for the EOS with a constant polytropic index the ordinary differential equation for Riemann invariants has not been integrated in analytical form [22], the use of the interpolated EOS ensures closed and simple analytical formulae for all Riemann invariants.

Here we consider 1D relativistic flow, depending upon the x-coordinate and the time t. All three components of velocity are taken into account.

As long as the particle number is conserved and the equation for the density is valid, the system of conservation laws, Eq. (8), has five Riemann invariants. Among them there are three invariants, propagating with a velocity $\lambda = v_x$,

$$\left(\frac{\partial}{\partial t} + v_x\frac{\partial}{\partial x}\right)\begin{pmatrix} h\gamma\mathbf{v}_\perp \\ \sigma \end{pmatrix} = 0, \tag{28}$$

where $\mathbf{v}_\perp = (v_y, v_z)$ are the velocity components which are normal to the x-axis, and σ is an entropy per unit of mass, or any monotone function of this. Further we denote $\mathbf{R}_\perp = h\gamma\mathbf{v}_\perp = \mathbf{J}_\perp/\rho$. Along the line $dx = v_x dt$ the differential of entropy is zero according to Eq. (28). Due to thermodynamic considerations, the equation $d\sigma = 0$ is equivalent to

$$r\,dh = d\,P. \tag{29}$$

On integrating the latter equation using the EOS Eqs. (16) and (20), one can represent the condition of entropy conservation along the line $dx = v_x dt$ as $dR_0 = 0$, where the Riemann invariant (an arbitrary monotone function of the entropy) may be chosen in the following way:

$$\tilde{\rho} = R_0 P^{1-2a}. \tag{30}$$

The adiabatic law, Eq. (30), coincides with that for nonrelativistic gas with a constant polytropic index κ on substituting $\frac{1}{1-2a} \to \kappa$ (see Eq. (23)).

In order to find two more Riemann invariants $R_\pm$ for perturbations, propagating with a sound velocity right and left hand side, respectively, one should consider a flow in which the other invariants are constant: $\mathbf{R}_\perp = const$, and $R_0 = const$. In isoentropic motion the gradient of pressure may be found as (see Eq. (29)) $\boldsymbol{\nabla} P = r \cdot \boldsymbol{\nabla} h$. As long as $\mathbf{R}_\perp = const$, the substitution $v_x = \tanh\xi$ gives also $\gamma v_x = \frac{h'}{h}\sinh\xi$ and $\gamma = \frac{h'}{h}\cosh\xi$, where

$$h' = \sqrt{h^2 + \mathbf{R}_\perp^2}. \tag{31}$$

With these denotations, the equations for density and velocity v_x (see Eqs. (8), (9)) may be written in a simple form as

$$\frac{\partial r'\cosh\xi}{\partial t} + \frac{\partial r'\sinh\xi}{\partial x} = 0, \tag{32}$$

$$\frac{\partial h'\sinh\xi}{\partial t} + \frac{\partial h'\cosh\xi}{\partial x} = 0, \tag{33}$$

where

$$r' = \tilde{\rho} h'. \tag{34}$$

This approach follows a way of solving the analogous problem in the particular case $\mathbf{R}_\perp = 0$ given in problem 1 following paragraph 134 in [1]. In this particular case all the *primed* variables in Eqs. (31), (34) coincide with *nonprimed* ones. Proceeding to the characteristic form of Eqs. (32), (33), one can readily find

$$\left(\frac{\partial}{\partial t} + \frac{v_x \pm c_s'}{1 \pm v_x c_s'}\frac{\partial}{\partial x}\right) R_\pm = 0, \quad dR_\pm = d\xi \pm \frac{dh'}{c_s' h'}, \tag{35}$$

where $R_\pm$ are the Riemann invariants which are transported at sound velocity with respect to the gas, where

$$c_s' = \left(\frac{r}{h}\frac{dh'}{dr'}\right)^{1/2} \tag{36}$$

is the speed of sound, transformed due to the transverse Doppler effect. The derivatives in Eqs. (35), (36) should be taken at the constant values of $\mathbf{R}_\perp$ and R_0. So using Eqs. (29), (31), (34), and (36) we can obtain two equivalent expressions for the sound velocity

$$(c_s')^{-2} = 1 + \frac{h'}{\tilde{\rho}}\frac{d\tilde{\rho}}{dh'} = 1 + (h')^2 \frac{d\tilde{\rho}}{dP} \tag{37}$$

and, using the first of these representations, derive a general formula for the increment of the Riemann invariant:

$$dR_\pm = d\xi \pm \frac{c_s' d\tilde{\rho}}{\left(1 - c_s'^{\,2}\right)\tilde{\rho}}. \tag{38}$$

This formula is valid for any EOS. In nonrelativistic limit it reduces to $dR_\pm = dv_x \pm c_s' d\tilde{\rho}/\tilde{\rho}$ and coincides with that for nonrelativistic hydrodynamics. Then the use of the interpolated EOS, Eq. (20), results in simple and efficient formulae for the sound speed,

$$(c_s')^{-2} = C_1^2(1 + 1/G), \tag{39}$$

where a constant C_1 and a combination of the hydrodynamical parameters G is introduced as follows:

$$C_1 = \sqrt{\frac{1-a}{a}}, \quad G = \frac{(1-a)P}{(1-2a)(a\mathbf{R}_\perp^2 + b)\tilde{\rho}}. \tag{40}$$

Now we can perform the integration of Eq. (38). From Eq. (30) we find $d\tilde{\rho}/\tilde{\rho} = (1 - 2a)dP/P$, and Eq. (39) gives $[ac_s' - (1-a)c_s'^{\,3}]dP/P = dc_s'$. The Riemann invariants may finally be found as

$$R_\pm = \xi \pm \left[\sqrt{\frac{1-a}{a}}\tanh^{-1}\left(\sqrt{\frac{1-a}{a}}c_s'\right) - \tanh^{-1} c_s'\right], \tag{41}$$

where the denotation $\tanh^{-1}(y) = \frac{1}{2}\log(\frac{1+y}{1-y})$ means inverse hype rbolic tangent, rather than $1/\tanh(y)$.

Thus we obtain direct analytical formulae for the Riemann invariants. They are simple and efficiently computable due to the use of the interpolated EOS. By comparing this with the results of [22], one can see that, using the EOS with a constant polytropic index, they obtained an ordinary differential equation for finding $R_\pm$ instead of our explicit equations Eq. (41). So instead of computing $R_\pm$ explicitly, in this case, it is necessary to integrate numerically the latter differential equation each time the Riemann invariant has to be calculated. The approach based on the interpolated EOS is much more efficient.

Using a formula $\tanh^{-1}(y) = \sinh^{-1}(y/\sqrt{1-y^2})$, one can rewrite Eq. (41) in the following form:

$$R_\pm = \xi \pm [C_1 \sinh^{-1}(\sqrt{G}) - \tanh^{-1} c_s']. \tag{42}$$

Equation (42) is useful for computations at very high values of pressure, when the sound velocity is so close to its limiting value $1/C_1$ so that the calculation of the first inverse hyperbolic tangent in Eq. (41) becomes impractical.

The incremental relation, Eq. (38), for the interpolated EOS may be used in a form as follows:

$$d R_\pm = d\xi \pm \frac{(1-2a)c_s'\, dP}{\left(1-c_s'^2\right)P}. \tag{43}$$

Within the Godunov scheme this formula should be used for finding the preliminary value of the pressure at the contact discontinuity to start the iteration procedure for finding a more accurate value for this.

6. SHOCK WAVES IN A GAS WITH AN INTERPOLATED EOS

Let us consider a shock wave with a front perpendicular to the axis x. All the velocity components are not equal to zero in the general case. It is important to emphasize that in choosing the frame of reference one can ensure that the perpendicular components of velocity become zero—but the shock wave front in this frame of reference generally is no longer perpendicular to the x-axis. Instead, let us choose a frame of reference moving along the x-axis with a velocity $D = \tanh(d)$ such that in this new frame of reference the front would be at rest (the equation of the front surface is $x = const$). The velocities in this new frame of reference are denoted by the upper index (D).

First, the Riemann invariants $\mathbf{R}_\perp = h\gamma\mathbf{v}_\perp$ not only remain continuous at the shock wave front, but they also do not change at the transition to a new frame of reference, because h is Lorenz invariant and $\gamma\mathbf{v}_\perp$ are transverse components of the 4-vector. For the x-component of the velocity the substitution $v_{x0,1} = \tanh(\xi_{0,1})$, $v_{x0,1}^{(D)} = \tanh(\xi_{0,1}^{(D)})$ is used. According to the relativistic law for the velocity addition, the values at the moving frame of reference are as follows:

$$\xi_{0,1}^{(D)} = \xi_{0,1} - d. \tag{44}$$

Equation (44) allows us to find the velocity of the shock wave and that of the gas behind the shock front

$$d = \xi_0 - \xi_0^{(D)}, \quad \xi_1 = \xi_0 - \xi_0^{(D)} + \xi_1^{(D)}, \tag{45}$$

the variables $\xi_0^{(D)}$ and $\xi_1^{(D)}$ being the functions of the shock wave intensity which are given by the Taub theory for relativistic shock waves [1].

According to this theory, the values of enthalpy and pressure h_1 and P_1 behind the shock wave front are connected by so-called Taub adiabat with the preshock values h_0 and P_0,

$$h_1^2 - h_0^2 = (P_1 - P_0)\left(\tilde{\rho}_1^{-1} + \tilde{\rho}_0^{-1}\right); \tag{46}$$

this relationship involves only Lorenz-invariant values, so it does not depend on the choice of the frame of reference. With the interpolated EOS one can readily find that $ah^2 = b + P/\tilde{\rho}$. Using this formula for representing the right-hand side of Eq. (44) in terms of P and $\tilde{\rho}$, one obtains

$$\tilde{\rho}_1 = \tilde{\rho}_0 \frac{(1-a)P_1 + aP_0}{aP_1 + (1-a)P_0}. \tag{47}$$

It is interesting to mention that on substituting $\tilde{\rho} \to \rho$ and $(1-2a)^{-1} \to \kappa$, the Eq. (47) fully coincides with the subsequent relationship for nonrelativistic gas with the constant polytropic index κ.

This analogy is also valid for the velocities ratio. Applying conservation laws for the energy and mass in a frame of reference, co-moving with a shock front

$$r_1\gamma_1^{(D)}v_{x1}^{(D)} = r_0\gamma_0^{(D)}v_{x0}^{(D)}, \quad h_1 r_1\left(\gamma_1^{(D)}\right)^2 v_{x1}^{(D)} = h_0 r_0\left(\gamma_0^{(D)}\right)^2 v_{x0}^{(D)}, \tag{48}$$

one can readily find (the first equation squared in Eq. (48) is divided by the second one)

$$\frac{v_{x1}^{(D)}}{v_{x0}^{(D)}} = \frac{\tilde{\rho}_0}{\tilde{\rho}_1} = \frac{aP_1 + (1-a)P_0}{(1-a)P_1 + aP_0}, \tag{49}$$

which is again in full accordance with the corresponding relationship for nonrelativistic shock waves in a gas with a constant polytropic index.

From the momentum conservation law

$$h_1 r_1\left(\gamma_1^{(D)}v_{x1}^{(D)}\right)^2 + P_1 = h_0 r_0\left(\gamma_0^{(D)}v_{x0}^{(D)}\right)^2 + P_0, \tag{50}$$

using Eqs. (48), one gets the formula for $v_{x0}^{(D)}$

$$\left(\gamma_0^{(D)}v_{x0}^{(D)}\right)^2 = \frac{P_1 - P_0}{r_0^2\left(\tilde{\rho}_0^{-1} - \tilde{\rho}_1^{-1}\right)} = \frac{(1-a)P_1 + aP_0}{(1-2a)r_0h_0}. \tag{51}$$

Taking into account the relationship $\gamma_0^{(D)}v_{x0}^{(D)} = \sqrt{1 + \mathbf{R}_\perp^2/h_0^2}\sinh(\xi_0^{(D)})$, one can finally obtain

$$\xi_0^{(D)} = \mp\sinh^{-1} c'_{s0}\sqrt{\frac{aP_0 + (1-a)P_1}{P_0\left(1 - c'^2_{s0}\right)}}; \tag{52}$$

here minus and plus are for the shock waves, moving to the right and left hand side, respectively. For weak shock waves, $P_1 \approx P_0$ and $\tanh \xi_0^{(D)} \approx \mp c'_{s0}$. For strong shock

waves, $\xi_0^{(D)} \to \infty$ and the velocity tends to the speed of light. In a quite analogous manner, the formula for $\xi_1^{(D)}$ is

$$\xi_1^{(D)} = \mp \sinh^{-1} c'_{s1} \sqrt{\frac{aP_1 + (1-a)P_0}{P_1\left(1 - c'^2_{s1}\right)}}. \tag{53}$$

At the limit of low temperature ($c'^2_{s1} \ll 1$, $\sinh \xi = v$, $a = b = \frac{\kappa - 1}{2\kappa}$) these formulae reduce to well-known relations for nonrelativistic gas (see [1], formulae Eq. (89.4)).

Thus, as long as the preshock parameters, such as $\tilde{\rho}_0$, P_0, and $\mathbf{R}^2_\perp$, as well as the pressure behind the front of shock wave P_1, are known, then one can find first $\tilde{\rho}_1$ using Eq. (47), then sound velocities, and after this the velocities d and ξ_1 using Eqs. (45), (52), and (53).

7. THE SOLUTION OF THE RIEMANN PROBLEM

The advantage of the exact formulae for the Riemann invariants is that in using these formulae one can construct exact, nonlinear, and explicit solutions of the CFD equations. These solutions, referred to as *simple* wave or Riemann wave solutions, may be obtained if all the Riemann invariants except one (either R_+ or R_-) are assumed to be constant. So the right simple wave is governed by the equations

$$\frac{\partial R_+}{\partial t} + \frac{v_x + c'_s}{1 + v_x c'_s} \frac{\partial R_+}{\partial x} = 0, \tag{54}$$

$$\xi + \tanh^{-1} c'_s(G) = R_{-R} + C_1 \sinh^{-1} \sqrt{G}, \tag{55}$$

where the index R marks the value of the Riemann invariants at some arbitrary state ("right state"), belonging to the right simple wave. Then, for the left wave, the analogous formulae become

$$\frac{\partial R_-}{\partial t} + \frac{v_x - c'_s}{1 - v_x c'_s} \frac{\partial R_-}{\partial x} = 0, \tag{56}$$

$$\xi - \tanh^{-1} c'_s(G) = R_{+L} - C_1 \sinh^{-1} \sqrt{G}. \tag{57}$$

In Eqs. (54–57) the sound velocity should be expressed in terms of G, using Eq. (39).

It is important to mention that the left-hand side of Eqs. (55) and (57) may be represented as $\tanh(\lambda_\pm)$, where $\lambda_\pm = (v_x \pm c'_s)/(1 \pm v_x c'_s)$ are the propagation velocities for the right and left waves correspondingly, which appear to be monotonic functions of pressure. In order for the simple waves not to break in the course of the time evolution, the propagation velocity should be a monotonic increasing function of the spatial coordinate x. We obtain that in the right simple wave, $p(x)$ should be an increasing function; in the left simple wave, $p(x)$, should be a decreasing function. In any case, the pressure increases toward the direction of propagation, which is why nonbreaking simple waves are always decompression waves. We do not use here the common term "rarefaction wave," because the dependence on the observable density ρ in the original frame of reference is sophisticated and is not discussed here.

An important particular simple decompression wave is the centered decompression wave, in which all the physical quantities depend upon time and spatial coordinates only in the

combination $\theta = x/t$. For the right wave, Eq. (54) gives, in this case

$$\theta = \frac{v_x + c'_s}{1 + v_x c'_s}, \tag{58}$$

so Eq. (55) allows us to exclude $v_x = \tanh(\xi)$ and find the spatial distribution of pressure, density, and sound velocity:

$$\mathbf{R}_\perp = \mathbf{R}_{\perp R}, \quad \frac{c'_s}{c'_{sR}}\sqrt{\frac{C_1^{-2} - c'^2_{sR}}{C_1^{-2} - c'^2_s}} = \left(\frac{\tilde{\rho}}{\tilde{\rho}_R}\right)^{\frac{a}{1-2a}} = \left(\frac{P}{P_R}\right)^a = \sqrt{\frac{G}{G_R}}, \tag{59}$$

$$\sqrt{G} = \sinh\left[C_1^{-1}(\tanh^{-1}\theta - R_{-R})\right]. \tag{60}$$

In the nonrelativistic limit Eq. (60) reduces to $c'_s = C_1^{-2}(\theta - v_{xR} - c'_{sR}) + c'_{sR}$ with $C_1^2 = \frac{\kappa+1}{\kappa-1}$ and conforms to the solution for the gas with a constant polytropic index.

When the sound speed is found, the velocity may then be obtained in the following way:

$$\xi = \tanh^{-1}\theta - \tanh^{-1} c'_s. \tag{61}$$

Two problems concerning the spatial distribution are of practical interest. First, the set of hydrodynamic parameters at some given value of θ and for the given right state may be directly obtained using Eq. (49). For example, let us assume that $\theta = 0$. On substituting the latter value in Eq. (60) one can find that in this state

$$\mathbf{R}_\perp = \mathbf{R}_{\perp R}, \quad \left(\frac{\tilde{\rho}}{\tilde{\rho}_R}\right)^{\frac{a}{1-2a}} = \left(\frac{P}{P_R}\right)^a = \frac{\sinh\left[-C_1^{-1}R_{-R}\right]}{\sqrt{G_R}}, \tag{62}$$

$$v_x = -c'_s. \tag{63}$$

Second, the velocity of the interface gas-vacuum may be found from Eqs. (60) and (61). At this interface the pressure and density both tend to zero, so that

$$\xi = \tanh^{-1}\theta = R_{-R}. \tag{64}$$

The solution of Eqs. (60) and (61) is defined only for the values of θ exceeding those satisfying the condition, Eq. (64). For lower values of θ the formula in Eq. (60) gives nonphysical negative values of density and pressure. Below we use Eqs. (62)–(64) within the Godunov scheme for various particular cases.

Now we have a set of exact nonlinear solutions for the relativistic CFD equations, namely the decompression simple waves and shock waves. Along with the contact discontinuity (CD), which does not require special consideration, being fully analogous to that in nonrelativistic CFD, this set is sufficient for constructing a solution of the Riemann problem for relativistic CFD equations.

The formulation of the problem is standard. At the time instant $t = 0$ the step-like initial condition is assumed for a 1D version of Eq. (8):

$$\frac{\partial \mathbf{U}(t,x)}{\partial t} + \frac{\partial \mathbf{F}(\mathbf{U})}{\partial x} = 0, \quad \mathbf{U}(0,x) = \mathbf{U}_L, x < 0, \quad \mathbf{U}(0,x) = \mathbf{U}_R, x > 0. \tag{65}$$

The initial conditions make sense only if the condition in Eq. (27) is fulfilled for both the two sets $\mathbf{U}_L$ and $\mathbf{U}_R$. In this case the two sets $\mathbf{U}_L$ and $\mathbf{U}_R$ define two sets of primitive variables $\mathbf{W}_L = (\tilde{\rho}_L, \xi_L, \mathbf{R}_{\perp L}, P_L)$ and $\mathbf{W}_R = (\tilde{\rho}_R, \xi_R, \mathbf{R}_{\perp R}, P_R)$. A solution of the problem is also given here via the primitive variables.

The solution of the Riemann problem is surely self-similar and depends on x, t only through the combination $\theta = x/t$. So the solution of the Riemann problem shown in Eq. (65) may be denoted as $\mathbf{U}_{RS}(\mathbf{W}_L, \mathbf{W}_R, \theta)$.

Let us begin with the case in which the differences in pressure and velocity are both small: $\xi_L \approx \xi_R$ and $P_L \approx P_R$. In this case the flow at $t > 0$ involves the CD and two step-like sound waves, propagating to the right-hand side and to the left-hand side outward from the CD. Let us find two sets of primitive variables at the left and right margins of the CD, $\mathbf{W}_L^{(c)} = (\tilde{\rho}_L^{(c)}, \xi^{(c)}, \mathbf{R}_{\perp L}^{(c)}, P^{(c)})$ and $\mathbf{W}_R^{(c)} = (\tilde{\rho}_R^{(c)}, \xi^{(c)}, \mathbf{R}_{\perp R}^{(c)}, P^{(c)})$, the pressure and x-component of the velocity as well as $\xi^{(c)}$ being continuous through the CD, as usual. In any case, $\mathbf{R}_{\perp M}^{(c)} = \mathbf{R}_{\perp M}$, $M = L, R$, here and below.

The sound wave propagating to the right is a particular case of a right simple wave. The relationship in Eq. (43) for the Riemann invariant R_- may be written for a small amplitude wave in the form of a finite increment relation:

$$\xi^{(c)} - \xi_R = \frac{(1-2a)c'_{sR}\left(P^{(c)} - P_R\right)}{\left(1 - c'^2_{sR}\right)P_R}. \tag{66}$$

In an analogous manner, for the left simple wave the relation for the invariant R_- gives

$$\xi_L - \xi^{(c)} = \frac{(1-2a)c'_{sL}\left(P^{(c)} - P_L\right)}{\left(1 - c'^2_{sL}\right)P_L}. \tag{67}$$

The sum of Eqs. (66) and (67) gives the equation for finding the pressure at the CD:

$$\xi_L - \xi_R = \frac{(1-2a)c'_{sR}\left(P^{(c)} - P_R\right)}{\left(1 - c'^2_{sR}\right)P_R} + \frac{(1-2a)c'_{sL}\left(P^{(c)} - P_L\right)}{\left(1 - c'^2_{sL}\right)P_L}. \tag{68}$$

It is important to mention that Eq. (68) involves the dependence on the right and left velocities only in the form of the dependence upon the relative velocity $\xi_L - \xi_R$. This point is a direct consequence of the relativistic invariance of relativistic CFD equations and in general is independent of the choice of the EOS and the assumption of small wave amplitudes.

On finding the pressure $P^{(c)}$ from the linear equation in Eq. (68), the full sets of hydrodynamic parameters at the CD may then be computed. This point is significant because the application of the linear approximation to the Riemann solver for sufficiently smooth numerical solutions is a usual practice resulting in higher efficiency. We see that this step is just as simple for the relativistic CFD equations as for nonrelativistic CFD.

So now we can proceed to the more difficult case, when the jumps in parameters are arbitrarily large.

The equation for finding the pressure at the CD is

$$\sum_{M=L,R} \Psi\left(P^{(c)}, P_M, \tilde{\rho}_M, \mathbf{R}_{\perp M}\right) = \xi_L - \xi_R, \tag{69}$$

where the function $\Psi(P^{(c)}, P_M, \tilde{\rho}_M, \mathbf{R}_{\perp M})$, $M = R, L$, can be found by combining

Eqs. (41) and (60) for $P^{(c)} < P_M$ as

$$\Psi\left(P^{(c)}, P_M, \tilde{\rho}_M, \mathbf{R}_{\perp M}\right) = C_1 \sinh^{-1}\left(\sqrt{G_M^{(c)}}\right) - \tanh^{-1} c_{sM}^{(c)} - C_1 \sinh^{-1}(\sqrt{G_M}) + \tanh^{-1} c_{sM}, \tag{70}$$

where the density near the CD is

$$\tilde{\rho}_M^{(c)} = \tilde{\rho}_M \left(P^{(c)}/P_M\right)^{1-2a}. \tag{71}$$

Then, for $P^{(c)} > P_M$ one should use the formula for $\Psi(P^{(c)}, P_M, \tilde{\rho}_M, \mathbf{R}_{\perp M})$, which comes from the Hugoniot relations in Eqs. (36), (37) as well as from Eq. (29):

$$\Psi\left(P^{(c)}, P_M, \tilde{\rho}_M, \mathbf{R}_{\perp M}\right) = \sinh^{-1} c_{sM} \sqrt{\frac{a + (1-a)P^{(c)}/P_M}{\left(1 - c_{sM}^2\right)}} - \sinh^{-1} c_{sM}^{(c)} \sqrt{\frac{a + (1-a)P_M/P^{(c)}}{\left(1 - \left(c_{sM}^{(c)}\right)^2\right)}}. \tag{72}$$

Density at the CD is given by Eq. (47):

$$\tilde{\rho}_M^{(c)} = \tilde{\rho}_M \frac{(1-a)P^{(c)} + aP_M}{aP^{(c)} + (1-a)P_M}. \tag{73}$$

The sound velocities $c_{sM}^{(c)}$ for both cases, $P^{(c)} > P_M$ and $P^{(c)} < P_M$, are expressed via $P^{(c)}$, $\tilde{\rho}_M^{(c)}$, and $\mathbf{R}_{\perp M}$ by Eq. (39).

The root of Eq. (69) can be readily found using the Newton–Raphson numerical procedure. An analogous algorithm is widely used in the Godunov numerical scheme implementations for nonrelativistic hydrodynamics and is published, for example, in [3]. The unique nonnegative solution for $P^{(c)}$ exists if a vacuum cavity does not form in the Riemann problem solution. The condition for this can be readily obtained by combining Eq. (64) and the analogous equation for the left decompression wave:

$$R_{+L} - R_{-R} \geq 0. \tag{74}$$

If Inequality (74) is not fulfilled, then without solving Eq. (69) one can construct the solution of the Riemann problem consisting of the two decompression waves and a vacuum cavity between them, the left and right gas-vacuum boundaries having the coordinates

$$\theta_L^{(c)} = \tanh R_{+L}, \quad \theta_R^{(c)} = \tanh R_{-R}, \tag{75}$$

respectively. Thus, the left decompression wave region is governed by the condition

$$\frac{v_L - c'_{sL}}{1 - v_L c'_{sL}} < \theta < \tanh R_{+L}, \tag{76}$$

while the right decompression wave is placed within the range of θ as follows:

$$\tanh R_{-R} < \theta < \frac{v_R + c'_{sR}}{1 + v_R c'_{sR}}. \tag{77}$$

On the contrary, if the condition in Eq. (74) is fulfilled and the numerical value of $P^{(c)}$ is obtained from Eq. (69), then the normal velocity of the CD can be found as

$$\xi^{(c)} = \xi_L - \Psi\left(P^{(c)}, P_L, \tilde{\rho}_L, \mathbf{R}_{\perp L}\right) = \xi_R + \Psi\left(P^{(c)}, P_R, \tilde{\rho}_R, \mathbf{R}_{\perp R}\right), \tag{78}$$

and the values of $\rho_M^{(c)}$ and $\mathbf{R}_{\perp M}$ are obtained in the course of determining the numerical solution of Eq. (69). Eq. (78) also gives the coordinate of the CD: $\theta^{(c)} = \tanh \xi^{(c)}$. Then the values of the hydrodynamic parameters in the solution of the Riemann problem can be found for any θ.

If $P^{(c)} > P_M$, then to the M-side of the CD there is a shock wave propagating outward from the CD. The shock wave front coordinate is (see Eq. (52))

$$\theta_{SW} = \tanh\left(\xi_M \pm \sinh^{-1} c'_{sM} \sqrt{\frac{a + (1-a)P^{(c)}/P_M}{\left(1 - c'^2_{sM}\right)}}\right), \tag{79}$$

where the sign $\pm$ is for $M = R, L$ respectively. The two constant hydrodynamic states $\mathbf{W}_M^{(c)} = (\tilde{\rho}_M^{(c)}, \xi^{(c)}, \mathbf{R}_{\perp M}^{(c)}, P^{(c)})$ and $\mathbf{W}_M = (\tilde{\rho}_M, \xi_M, \mathbf{R}_{\perp M}, P_M)$ are connected through the shock front.

If $P^{(c)} < P_M$ then the decompression wave propagates to the M-side outward from the CD, connecting the two constant hydrodynamic states $\mathbf{W}_M^{(c)} = (\tilde{\rho}_M^{(c)}, \xi^{(c)}, \mathbf{R}_{\perp M}^{(c)}, P^{(c)})$ and $\mathbf{W}_M = (\tilde{\rho}_M, \xi_M, \mathbf{R}_{\perp M}, P_M)$. The decompression wave region is governed by the condition

$$\frac{\tanh \xi^{(c)} + c'^{(c)}_{sR}}{1 + \tanh \xi^{(c)} c'^{(c)}_{sR}} < \theta < \frac{v_R + c'_{sR}}{1 + v_R c'_{sR}} \tag{80}$$

for $M = R$ and/or

$$\frac{v_L - c'_{sL}}{1 - v_L c'_{sL}} < \theta < \frac{\tanh \xi^{(c)} - c'^{(c)}_{sL}}{1 - \tanh \xi^{(c)} c'^{(c)}_{sL}} \tag{81}$$

for $M = L$. The spatial distribution of the hydrodynamic parameters within the decompression waves is given by Eqs. (59), (60).

Thus the full solution of the Riemann problem is described here. For the given left and right hydrodynamic states $\mathbf{U}_L$, $\mathbf{U}_R$ satisfying the condition in Inequality (74), only one simple transcendent equation, Eq. (69), should be numerically solved for finding the pressure at the CD. After this the hydrodynamic parameters for any given θ can be found.

8. GODUNOV SCHEME AND TEST RESULTS

As long as the numerical procedure for constructing the exact Riemann solver is found, the first order Godunov scheme may be formulated in the usual way [2, 3]. Consider the simplest case of a 1D problem at an equally spaced grid (Δx). The conserved variables averaged over the ith control volume $\mathbf{U}_i^n$ may be updated through a time step Δt, satisfying

the Courant–Friedrichs–Levi (CFL) stability condition, by using a standard finite volume method,

$$\mathbf{U}_i^{n+1} = \mathbf{U}_i^n + \frac{\Delta t}{\Delta x}\left(\mathbf{F}_{i-1/2} - \mathbf{F}_{i+1/2}\right), \tag{82}$$

where the numerical flux for the Godunov scheme is

$$\mathbf{F}_{i-1/2} = \mathbf{F}(\mathbf{U}_{RS}(\mathbf{W}_{i-1}, \mathbf{W}_i, 0)), \tag{83}$$

with $\mathbf{U}_{RS}(\mathbf{W}_L, \mathbf{W}_R, \theta)$ again being the solution of the Riemann problem, as denoted above, and $\mathbf{W}_i = \mathbf{W}(\mathbf{U}_i^n)$.

Let us consider the procedure for computing the first order numerical flux, step by step. The sets of the conserved variables U_i^n and U_{i+1}^n are employed to find the numerical flux $F_{i+1/2}$ as left and right hydrodynamic states. The transverse invariants $\mathbf{R}_\perp = \mathbf{J}_\perp/\rho$ can be found immediately.

Then the values of pressure as well as the values of Π should be recovered for both sets using Eq. (24), as long as the interpolated EOS is used. Otherwise the general equation in Eq. (12) should be solved for both the conserved variable sets.

After finding Π, the density $\tilde{\rho}$ may be found using Eqs. (10). The normal component of the velocity can also be found from Eqs. (13), or even better, the values of the parameter $\xi = \sinh^{-1}(J_x/(\Pi^2 - J_x^2))$ can be calculated.

To apply the exact Riemann solver, the constants a and b should be known. They can be chosen in advance for all the computational domains, if the interpolated EOS is used; otherwise the values of these constants should be chosen separately for each face of the control volume depending on the hydrodynamic states in the adjacent cells. Although the latter method is possible, we used only $a = b = 1/4$ in all the test computations.

Then the procedure for computing the primitive variables set $\mathbf{W}$ "at the face" (at $\theta = 0$) is straightforward. On solving Eq. (69) numerically one can find the sets of primitive variables $\mathbf{W}_M^{(c)}$ at the CD. Then depending upon the signs of different characteristic velocities, the state at $\theta = 0$ may coincide with $\mathbf{W}_M^{(c)}$ or $\mathbf{W}_M$. The only case in which some additional computations are needed arises if the coordinate value $\theta = 0$ belongs to the decompression wave. In this case, the values of the primitive variables are calculated using the formulae in Eqs. (62). If the condition Inequality (74) is violated, then the line $\theta = 0$ may also appear to be inside of the vacuum cavity, resulting in a zero numerical flux.

Then the conserved variables should be recovered for the state at the face and the numerical flux $\mathbf{F}_{i-1/2}$ may be calculated. After all, the formula in Eq. (82) with the calculated numerical fluxes allows us to update the numerical solution $\mathbf{U}_i$ through one time step.

The results for the first order test simulation are shown in Fig. 2 by the triangular symbols. The 1D computational domain $0 \le x \le 1$ consists of 100 cells; the initial state was $\rho = 1$, $\mathbf{v} = 0$, and $P = 2$ for $0 \le x \le 0.5$, $P = 1$ for $0.5 \le x \le 1$. In all the tests the time step was chosen according to the CFL stability condition with the CFL number $CFL = 0.7$. The density distribution for the time instant $t = 0.7$ is presented. The first order numerical solution is stable and monotone, but of course its accuracy is not sufficient for practical purposes.

The way to get the second order extension of the Godunov scheme is ambiguous. We apply the scheme proposed in [27]. Here we follow the formulation given in [28]. According to the terminology used in [3], the scheme may also be referred to as the MUSCL–Hancock scheme.

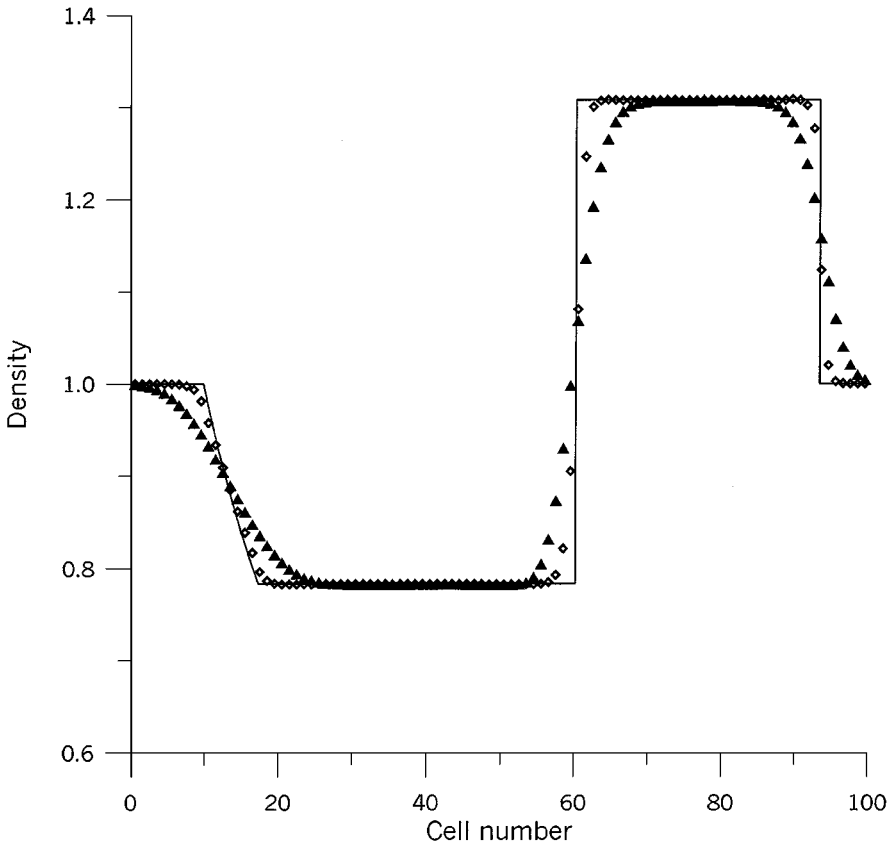

FIG. 2. The result of a 1D test simulation for a shock tube problem. Triangular symbols are the simulation results for the first order Godunov scheme; diamonds are the same for the second order scheme; and the line is a theoretical distribution obtained from the solution of the Riemann problem.

The two step predictor–corrector scheme is constructed in the following way. In order to achieve second order spatial accuracy, the spatial differences of the primitive variables are calculated and limited for each control volume,

$$\delta \mathbf{W}_i = \frac{1}{2} L(\mathbf{W}_{i+1} - \mathbf{W}_i, \mathbf{W}_i - \mathbf{W}_{i-1}), \tag{84}$$

where the limiter function $L(a, b)$ is applied to obtain nonoscillating numerical solutions. The symmetric β-limiter function which is described in [2, Eq. (21.3.35), p. 543] is used. To achieve second order temporal accuracy, one can calculate first the predicted values of the conserved variables:

$$\tilde{\mathbf{U}}_i^n = \mathbf{U}_i^n + \frac{\Delta t}{\Delta x}\big(\mathbf{F}\big(\mathbf{W}_i^n - \delta \mathbf{W}_i\big) - \mathbf{F}\big(\mathbf{W}_i^n + \delta \mathbf{W}_i\big)\big). \tag{85}$$

After this the predicted values for the primitive variables are recovered: $\tilde{\mathbf{W}}_i = \mathbf{W}(\tilde{\mathbf{U}}_i^n)$. Then the second order numerical flux is calculated as

$$\mathbf{F}_{i-1/2} = \mathbf{F}\left(\mathbf{U}_{RS}\left(\frac{1}{2}\mathbf{W}_{i-1} + \frac{1}{2}\tilde{\mathbf{W}}_{i-1} + \delta \mathbf{W}_{i-1}, \frac{1}{2}\mathbf{W}_i + \frac{1}{2}\tilde{\mathbf{W}}_i - \delta \mathbf{W}_i, 0\right)\right), \tag{86}$$

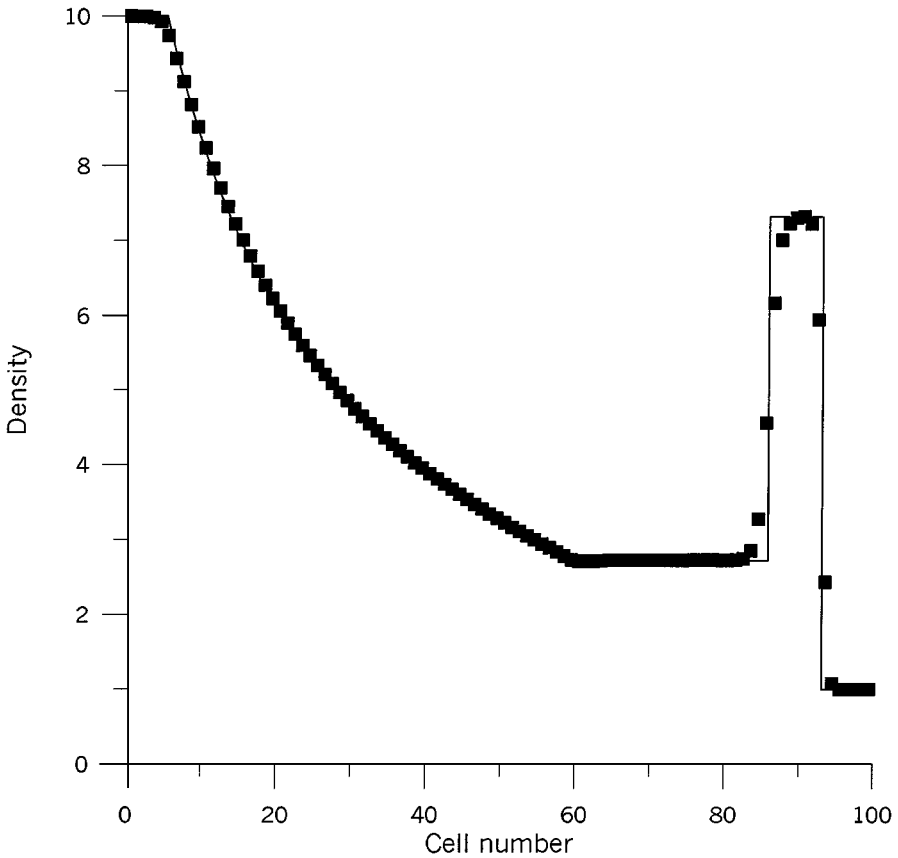

FIG. 3. The result of a 1D test simulation for a shock tube problem with a stronger shock wave, second order scheme.

which allows us to update the numerical solution using the general conservative numerical scheme in Eq. (82).

For the same test problem as treated above using the first order scheme, the results are shown in Fig. 2 (diamond symbols). The resolution is reasonably improved.

The results for the test problem with a stronger shock wave are given in Fig. 3. The initial conditions for a shock tube problem ($\mathbf{u} = 0$) are chosen as follows: $P = 100$, $\rho = 10$ for the left constant state; $P = 1$, $\rho = 1$ for the right state. The initial position of the discontinuity is between 40 and 41 zones ($x = 0.4$), and the total number of zones is 100. The value of β in a limiter function is $\beta = 1.7$. The simulation data for the density are given for the time instant $t = 0.6$ and the exact solution for the corresponding Riemann problem is shown for a comparison. The quality of the test results seems to be sufficiently high.

To compare the quality of the numerical results with those obtained, for example, in [29, 30], we also performed the simulation for a test above with a greater jump in pressure: $P = 13.3$ at $0 \le x \le 0.4$ and $P = 10^{-6}$ at $0.4 \le x \le 1$, the jump in density being the same. This test problem was treated in [29, 30] for the EOS in Eq. (18) with $\kappa = 5/3$. With our EOS and $a = b = 1/4$ this test is more demanding since the jumps in the density at the shock wave front and at the CD are stronger in our case, but the difference is not too essential. To compare the results we increased the number of zones to 200, as in [30], although our

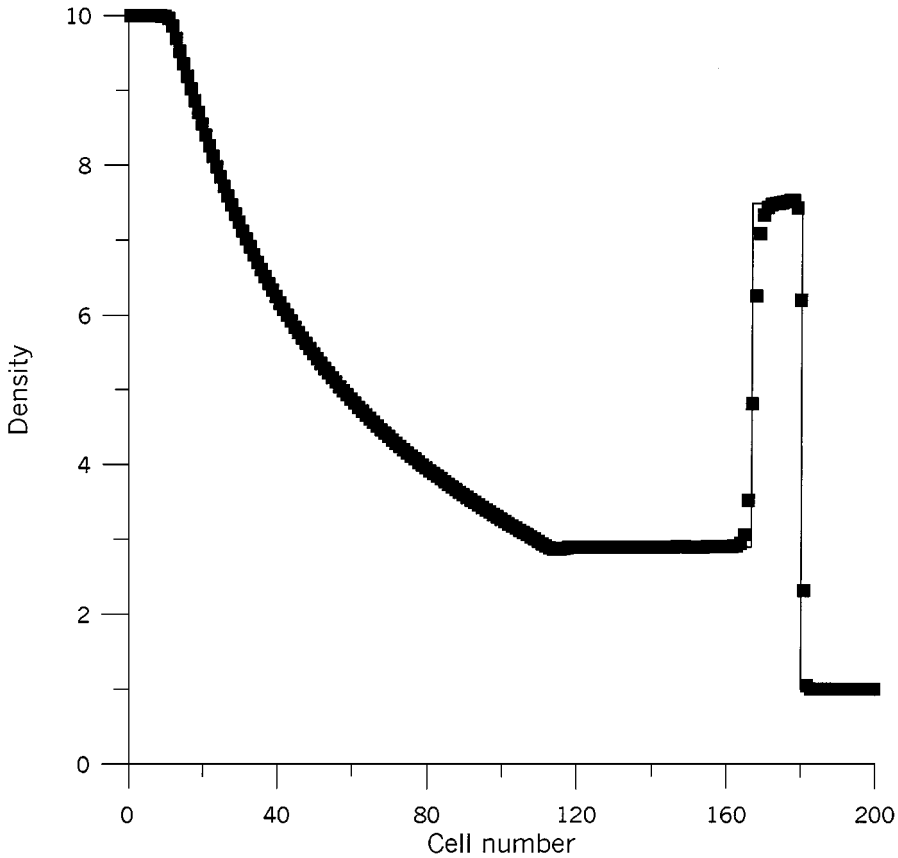

FIG. 4. The result for the test considered in [29, 30].

resolution for 100 zones appears sufficient. Rough comparison shows that the jumps are better resolved when the Godunov scheme with the exact Riemann solver is used (see Fig. 4 and analogous figures in [29, 30]).

To check the computational efficiency we also performed a 2D simulation for a relativistic jet. Through the upper boundary of the rectangular computational volume (see Fig. 5), the jet is injected starting from the initial time instant $t = 0$. The computational volume is $400\Delta \times 750\Delta$; the jet width is 40Δ. The jet speed is $0.995c$, which corresponds to a Lorenz factor $\gamma \approx 10$. The jet is injected into a gas with a density $\rho_m = 450$ while the jet density *in the original frame of reference* is $\rho_j = 45$. The pressure is assumed to be very low in both the ambient medium and the injected jet ($P = 0.01$).

The density distribution is displayed in Fig. 5 for a time instant $t = 1300\Delta/c$. The resolution of the vortex-shock structure in the head of the jet and the Kelvin–Helmholtz instability at the jet surface and at the cocoon boundary is good enough. To compare the results with the numerous publications on relativistic jet simulation see, e.g., [31] and the papers cited there, as well as [33]. The "dangerous" temperature $P/r \sim 0.1$ at which the quantitative accuracy of the interpolated EOS is not very good exists only within the head shock wave front, because behind the shock wave and in the jet matter the temperature is significantly higher, and in front of the shock wave the matter is cold and the input from the thermal energy is negligible. It should be mentioned that within the shock front ideal

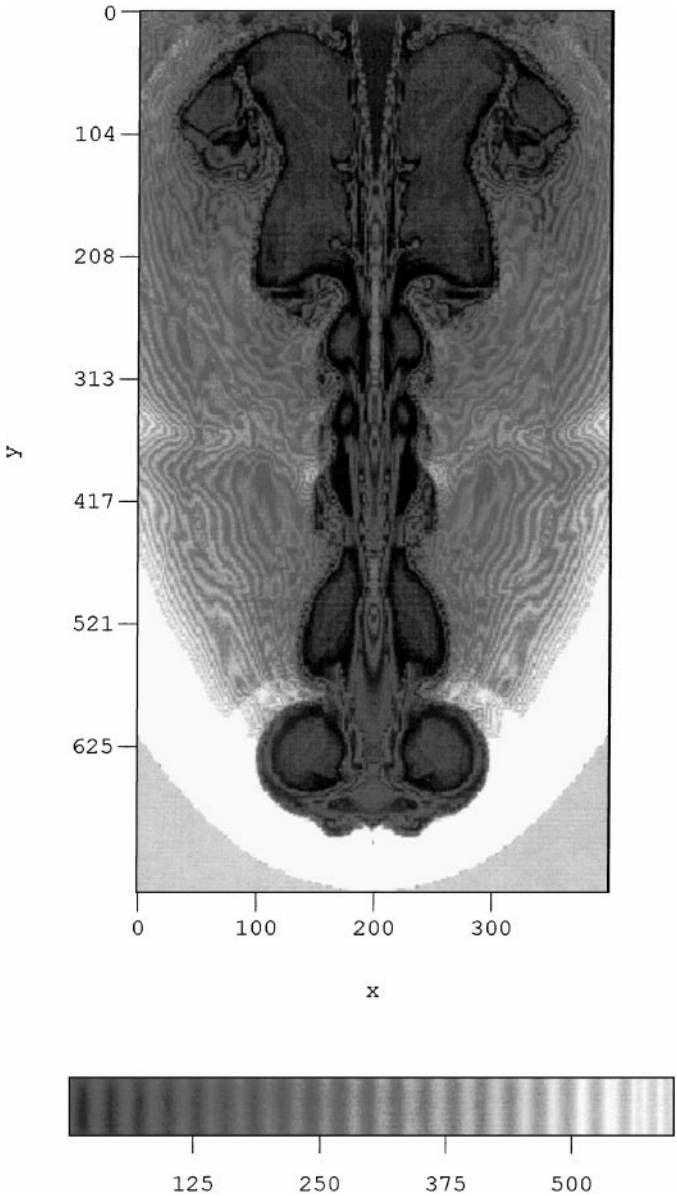

FIG. 5. The density pattern produced by a relativistic jet propagation through a dense medium. For better resolution of the distribution details we show all the density levels which exceed the value $\rho_{lim} = 600$ in white; actually the maximum density is $\rho_{max} \approx 1.8 \cdot 10^3$, while the density grey-scale in the figure is restricted by the value ρ_{lim}.

hydrodynamics is not applicable, so that the choice of an EOS for the matter inside of the front is meaningless.

Using a Pentium III 400 desktop computer we get better performance (10^{-5} sec per cell per time step) in this 2D test than is usually achieved with big computers.

Thus the second order Godunov scheme is simple and efficient. It allows us to use reasonably large values of the time step ($CFL = 0.7$–0.8) and to obtain high-quality results using a moderate desktop computer.

The programing task is trivial; actually we have used the existing code based on the second order Godunov scheme for *nonrelativistic CFD* and have transformed it code for the relativistic CFD by making minor changes.

9. CONCLUSION

We constructed a simple and efficient Godunov scheme for relativistic CFD. A key point is to make an appropriate choice of an approximation for the equation of state of matter at relativistic temperatures.

ACKNOWLEDGMENTS

We are grateful to Dr. E. Timofeev for useful discussions, and to Professor N. Cramer for numerous comments. We also thank Professor Ph. A. Hughes for reprints of papers.

REFERENCES

1. L. D. Landau and E. M. Lifshitz, *Gydrodinamica/Hydrodynamics* (Nauka, Moscow, 1986), [In Russian].
2. C. Hirsch, *Numerical Computation of Internal and External Flows. Vol. 2: Computational Methods for Inviscid and Viscous Flows* (Wiley, Chichester 1990), p. 132.
3. E. F. Toro, *Riemann Solvers and Numerical Methods for Fluid Dynamics* (Springer-Verlag, Berlin, 1997).
4. I. V. Sokolov, Computational relativistic hydrodynamics as applied for simulations of strong laser pulses and relativistic cumulative jets, in *Proceedings of the 30th Annual Anomalous Absorption Conference, Ocean City MD* (2000), p. 79.
5. R. D. Blandford and M. J. Rees, A "twin-exhaust" model for double radio sources, *Mon. Not. R. Astron. Soc.* **169**, 395 (1974).
6. M. L. Norman, K.-H. A. Winkler, and M. D. Smith, Structure and dynamics of supersonic jets, *Astron. Astrophys.* **113**, 285 (1982).
7. M. L. Norman and K.-H. A. Winkler, *Astrophysical Radiation Hydrodynamics*, edited by M. J. Norman and K.-H. A. Winkler (Reidel, Dordrecht, 1986), p. 449.
8. D. Kössl and E. Müller, Numerical simulations of astrophysical jets—The influence of boundary conditions and grid resolution, *Astron. Astrophys.* **206**, 204 (1998).
9. M. L. Norman, *Astrophysical Jets*, edited by D. Burgarella, M. Livio, and C. O'Dea (Cambridge Univ. Press, Cambridge, UK, 1993), p. 211.
10. J. R. Wilson, *Sources of Gravitational Radiation*, edited by L. Smarr (Cambridge Univ. Press, Cambridge, UK, 1979), p. 423.
11. P. R. Woodward, PPM: Piecewise-parabolic methods for astrophysical fluid dynamics, in *Astrophysical Radiation Hydrodynamics*, edited by M. J. Norman and K.-H. A. Winkler (Reidel, Dordrecht, 1986), p. 245.
12. J. M^a. Martí, E. Müller, and J. M^a. Ibáñez, Hydrodynamical simulations of relativistic jets, *Astron. Astrophys.* **281**, L9 (1994).
13. G. C. Duncan and P. A. Hughes, Simulations of relativistic extragalactic jets, *Astrophys. J. Lett.* **436**, L119 (1994).
14. J. M^a. Martí, E. Müller, J. A. Font, and J. M^a. Ibáñez, Morphology and dynamics of highly supersonic relativistic jets, *Astophys. J. Lett.* **448**, L105 (1995).
15. M. A. Aloy, J. M^a. Ibáñez, J. M^a. Martí, and E. Müller, GENESIS: A high-resolution code for three-dimensional relativistic hydrodynamics, *Astrophys. J. Suppl.*, **122**, 151 (1999).
16. S. Siegler and H. Riffert, Simulations of ultrarelativistic shocks, *Astrophys. J.* **531**, 1053 (2000).
17. J. A. Font, Numerical hydrodynamics in general relativity, in *living review in relativity*, available at http:/www.livingreviews.org/Articles/3 (2000).

18. L. Wen, A. Panaitescu, and P. Laguna, A shock-patching code for relativistic fluid flows, *Astrophys. J.* **486**, 919 (1997).
19. S. A. E. G. Falle and S. S. Komissarov, An upwind numerical scheme for relativistic hydrodynamics with a general equation of state. *Mon. Not. R. Astron. Soc.* **278**, 586 (1996).
20. S. Koide, K. I. Nishikawa, and R. L. Mutel, A Two-dimensional simulation of a relativistic magnetized jet, *Astrophys. J. Lett.* **463**, L71 (1996).
21. J. M^a. Martí and E. Müller, The analytical solution of the Riemann problem in relativistic hydrodynamics, *J. Fluid Mech.* **258,** 317 (1994).
22. J. Pons, J. M^a. Martí, and E. Müller, An exact Riemann solver for multidimensional special relativistic hydrodynamics, available at *astro-ph/991046* (1999).
23. L. D. Landau and E. M. Lifshitz, *Statisticheskaia Fizika/Statistical Physics* (Nauka, Moscow, 1976), [In Russian].
24. S. Chandrasekhar, *An Introduction to the Study of Stellar Structure* (Dover, New York, 1958).
25. G. C. Duncan, P. A. Hughes, and J. Opperman, Simulations of relativistic extragalactic jets: a variable equation of state, in *Energy Transport in Radio Galaxies and Quasar* (ASP Conf. Ser. Vol. 100), edited by P. E. Hardee, A. H. Bridle, and J. A. Zensus, pp. 143–148 (Astron. Soc. of the Pacific, 1996).
26. B. Einfeld, C. D. Munz, P. L. Roe, and B. Sjoegreen, On Godunov-type methods near low densities, *J. Comput. Phys.* **92**, 273 (1991).
27. A. V. Rodionov, Improvement of the approximation order in the Godunov scheme. *Zh. Vychisl. Mat. Mat. Piz.* **27**, 1853 (1987).
28. A. A. Fursenko, N. P. Mende, K. Oshima, D. M. Sharov, E. V. Timofeev, and P. A. Voinovich, Numerical simulation of propagation of shock waves through channel bends, *Comput. Fluid Dyn.* **2**, 1 (1993).
29. J. M^a. Martí and E. Müller, Extension of the piecewise parabolic method to one-dimensional relativistic hydrodynamics, *J. Comput. Phys.* **123**, 1 (1996).
30. R. Donat, J. A. Font, J. M^a. Ibáñez, and A. Marquina, A flux-split algorithm applied to relativistic flows, *J. Comput. Phys.* **146**, 56 (1998).
31. E. Müller, Simulation of astrophysical fluid flow, in *Computational Methods for Astrophysical Fluid Flow* (Springer-Verlag, Berlin/New York, 1998), p. 343.
32. P. A. Hughes, Confronting hydrodynamic simulations of relativistic jets with data: What do we learn about particles and fields? preprint available at *astro-ph/0011127*, (2000); in *Particles and Fields in Radio Galaxies ASP Conf. Ser.* (2001), to appear.
33. H.-M. Zhang, S. Koide, and J. I. Sakai, Two-dimensional simulation of relativistic jet-cloud collisions, *Publ. Astron. Soc. Japan* **51**, 449 (1999).